Available online at www.sciencedirect.com
ScienceDirect
International Journal of Heat and Mass Transfer 49 (2006) 4795–4803
International Journal of HEAT and MASS TRANSFER
www.elsevier.com/locate/ijhmt

Three-dimensional convection flow adjacent to inclined backward-facing step

Y.T. Chen *, J.H. Nie, H.T. Hsieh, L.J. Sun

Department of Mechanical Engineering, University of Nevada, Las Vegas, NV 89154, USA

Received 27 January 2006; received in revised form 3 June 2006
Available online 17 August 2006

Abstract

Simulations of three-dimensional laminar forced convection adjacent to inclined backward-facing step in rectangular duct are presented to examine effects of step inclination on flow and heat transfer distributions. The step height is maintained as constant while its inclination angle is changed from 15° to 90°. The inlet flow is hydrodynamically steady and fully developed with uniform temperature. The bottom wall is heated with constant heat flux, while other walls are maintained as being thermally adiabatic. Velocity, temperature, Nusselt number, and friction coefficient distributions are presented. The "jet-like" flow and its impingement do not appear as the inclination angle of backward-facing step is small ($\alpha = 15°$). At the center width of the duct and close to the stepped wall, the location where the streamwise velocity component is zero changes from a saddle point to a nodal point as the step inclination angle decreases. The downwash adjacent to the sidewall becomes stronger as the step inclination angle increases. The maximum Nusselt number on the stepped wall is located near the sidewall for $\alpha \geqslant 30°$ and it appears near the center width of duct for small step inclination angle ($\alpha = 15°$). The friction coefficient inside the primary recirculation region increases with the increase of the step inclination angle. Downstream of the primary recirculation region, increase of the friction coefficient becomes slower as the step inclination angle increases.

1. Introduction

Separating and reattaching flows because of sudden change in flow geometry occur in a wide variety of practical engineering applications such as power generating equipment, diffuser, electronic and turbine blade cooling, combustor, sudden area change in pipes or ducts, and atmospheric flows over fences and hills. A great deal of mixing of high and low energy fluid occurs in the flow reattachment region, thus impacting significantly the flow and heat transfer performance of these devices. In particular, thermal and momentum transports in the reattaching flow region and inside the reverse flow regions vary greatly. For example, the minimum wall shear stress and the maximum heat transfer rate occur in the neighborhood of reattaching flow region, while the minimum heat transfer rate occurs at the corner where the sudden change in geometry starts. Most of these industrial applications exhibit three-dimensional (3-D) behavior but most of the published studies are restricted to the two-dimensional (2-D) case. Fundamental features of this class of flows have been addressed most frequently for the backward-facing step, in which the separation line is straight and fixed by the geometry. This geometry is very simple, yet the flow and the heat transfer through it contain most of the complexities that are encountered in other separating flow geometries. The size of the reverse flow region characterizes the global features of flow and heat transfer in this geometry, and it has been used in benchmark studies for validating two-dimensional simulation algorithms/codes and equipment (see, for example, [1–3] and the references cited therein). Simulations and measurements of flow adjacent to the 2-D backward-facing step geometry have appeared extensively in the

* Corresponding author.
E-mail address: uuchen@nscee.edu (Y.T. Chen).

0017-9310/$ - see front matter © 2006 Elsevier Ltd. All rights reserved.
doi:10.1016/j.ijheatmasstransfer.2006.06.014

Nomenclature

AR	aspect ratio $= W/S$
C_f	skin friction coefficient $= 2\tau_w/\rho u_0^2$
C_p	specific heat
ER	expansion ratio $= H/(H-S)$
H	duct height downstream of the step
h	duct height upstream of the step
k	thermal conductivity
L	half width of the duct
Nu	Nusselt number $= q_w S/k(T_w - T_0)$
p	pressure
q_w	wall heat flux $= -k\partial T/\partial y\|_{\text{at the wall}}$
Re	Reynolds number $= 2\rho u_0 h/\mu$
S	step height
T	temperature
T_0	inlet temperature
T_w	wall temperature
u	velocity component in the x-coordinate direction
u_0	average inlet velocity
v	velocity component in the y-coordinate direction
W	width of the duct
w	velocity component in the z-coordinate direction
x	streamwise coordinate direction
x_s	location of the step edge on the stepped wall
x_u	locations where the streamwise velocity gradient is zero ($\partial u/\partial y = 0$)
y	transverse coordinate direction
z	spanwise coordinate direction

Greek symbols

α	inclination angle of the step
μ	dynamic viscosity
ρ	density
τ_w	wall shear stress $= \mu\sqrt{(\partial u/\partial y)^2 + (\partial w/\partial y)^2}$

literature [4–6], but limited results have been published on the 3-D flow adjacent to this geometry.

Simulations of 3-D separated-reattached flow adjacent to backward-facing step by Chiang and Sheu [7,8], by Iwai et al. [9], and by Carrington and Pepper [10] revealed some of the complex laminar flow behaviors that develop in this geometry. Armaly et al. [11] illustrated the developments of a downwash adjacent to the sidewall, followed with swirling spanwise flow inside the primary reverse flow region, and a swirling "jet-like" flow that impinges on the stepped wall near the sidewall in this geometry. The strong spanwise flow that develops adjacent to the stepped wall makes it difficult to identify the reattachment region of this separated-reattached 3-D flow, as noted by Nie and Armaly [12]. Effects of aspect ratio [9], step height [13], and Reynolds number [14] on three-dimensional separated-reattached convection flow adjacent to backward-facing step are examined. Mixed convection flow in this geometry was reported by Iwai et al. [15], by Li and Armaly [16], and recently by Saldana et al. [17]. All of these numerical and/or experimental studies brought to light the complex characteristics of flow and heat transfer in this geometry.

Majority of the previous work focuses on the configuration that the backward-facing step is vertical to the stepped wall. To the best of the authors' knowledge, study of three-dimensional fluid flow and heat transfer adjacent to inclined backward-facing step has not been seen in the published literature. This fact, along with the realization that such a geometry with inclined step configuration appears regularly in many industrial heat transfer devices, such as the combustion chamber, the transition duct connection, and others, motivated the present study.

2. Model description and simulation

Three-dimensional laminar forced convection flow in a heated rectangular duct with an inclined backward-facing step is numerically simulated, and a schematic of the computational domain is shown in Fig. 1. The upstream height of the duct (h) is 0.01 m, its downstream height (H) is 0.02 m, and its width (W) is 0.08 m. This geometry provides a backward-facing step height (S) of 0.01 m, an expansion ratio of ER $= H/(H-S) = 2$, and an aspect ratio of AR $= W/S = 8$. The selection of the values for these parameters is motivated by the fact that laser-Doppler measurements [18] are available for this geometry and they can be used to validate the flow simulation code. By exploiting the symmetry of the flow field in the spanwise direction, the width of the computational domain is reduced to half of the actual width of the duct ($L = W/2 = 0.04$ m). The length of the computational domain is 0.02 m and 0.5 m upstream and

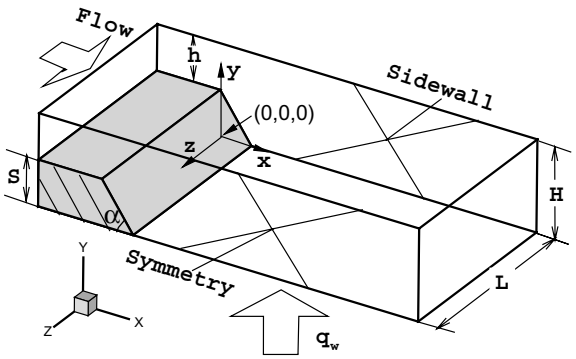

Fig. 1. Schematic of the computational domain.

downstream of the sudden expansion respectively, i.e., $-2 \leqslant x/S \leqslant 50$. This choice is made to ensure that the flow at the inlet section of the duct ($x/S = -2$) is not affected significantly by the sudden expansion in the geometry at the step, and the flow at the exit section ($x/S = 50$) is fully developed. It was confirmed that the use of a longer computational domain did not change the flow behavior in the region close to the backward-facing step ($x/S < 15$). Velocity measurements in the same geometry at $\alpha = 90°$ show that the flow is laminar and steady for Reynolds number (Re) smaller than 500 [18]. The steady laminar three-dimensional Navier–Stokes and energy equations are solved numerically (using finite volume scheme) together with the continuity equation to simulate the thermal and the flow fields.

Continuity equation:

$$\frac{\partial}{\partial x}(\rho u) + \frac{\partial}{\partial y}(\rho v) + \frac{\partial}{\partial z}(\rho w) = 0 \tag{1}$$

Momentum equations:

$$\frac{\partial}{\partial x}(\rho uu) + \frac{\partial}{\partial y}(\rho uv) + \frac{\partial}{\partial z}(\rho uw) = -\frac{\partial p}{\partial x} + \mu\left(\frac{\partial^2 u}{\partial x^2} + \frac{\partial^2 u}{\partial y^2} + \frac{\partial^2 u}{\partial z^2}\right) \tag{2}$$

$$\frac{\partial}{\partial x}(\rho uv) + \frac{\partial}{\partial y}(\rho vv) + \frac{\partial}{\partial z}(\rho vw) = -\frac{\partial p}{\partial y} + \mu\left(\frac{\partial^2 v}{\partial x^2} + \frac{\partial^2 v}{\partial y^2} + \frac{\partial^2 v}{\partial z^2}\right) \tag{3}$$

$$\frac{\partial}{\partial x}(\rho uw) + \frac{\partial}{\partial y}(\rho vw) + \frac{\partial}{\partial z}(\rho ww) = -\frac{\partial p}{\partial z} + \mu\left(\frac{\partial^2 w}{\partial x^2} + \frac{\partial^2 w}{\partial y^2} + \frac{\partial^2 w}{\partial z^2}\right) \tag{4}$$

Energy equation:

$$\frac{\partial}{\partial x}(\rho C_p uT) + \frac{\partial}{\partial y}(\rho C_p vT) + \frac{\partial}{\partial z}(\rho C_p wT) = k\left(\frac{\partial^2 T}{\partial x^2} + \frac{\partial^2 T}{\partial y^2} + \frac{\partial^2 T}{\partial z^2}\right) \tag{5}$$

where T is temperature, and u, v, w are velocity components in coordinate directions of x, y, and z as shown in Fig. 1 in this geometry. The physical properties are treated as constants in the simulation and evaluated for air at the inlet temperature of $T_0 = 20$ °C (i.e., density (ρ) equals to 1.205 kg/m^3, dynamic viscosity (μ) is 1.81×10^{-5} kg/m s, thermal conductivity (k) is 0.0259 W/m °C, and specific heat (C_p) is 1005 J/kg °C). The boundary conditions are treated as no slip conditions at the solid walls (zero velocities), and thermally adiabatic at all the walls with the exception of the downstream stepped wall ($y/S = 0.0$, for $x_s \leqslant x/S \leqslant 50$ and all z, where x_s is the step edge on the stepped wall) that was treated as having a fixed and uniform heat flux ($q_w = -k\partial T/\partial y|_{y=0}$) that is equal to $q_w = 50$ W/m^2. The flow rate was maintained at constant

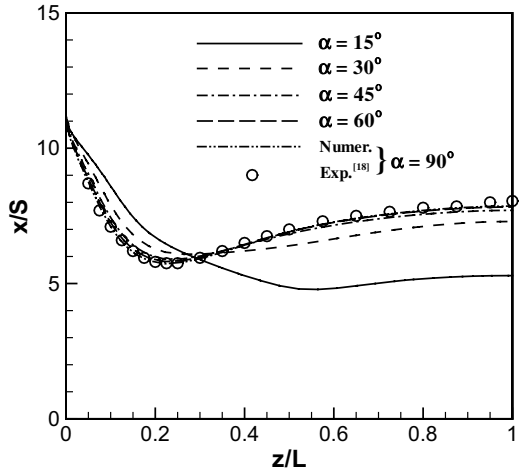

Fig. 2. Distribution of the x_u-lines on the stepped wall.

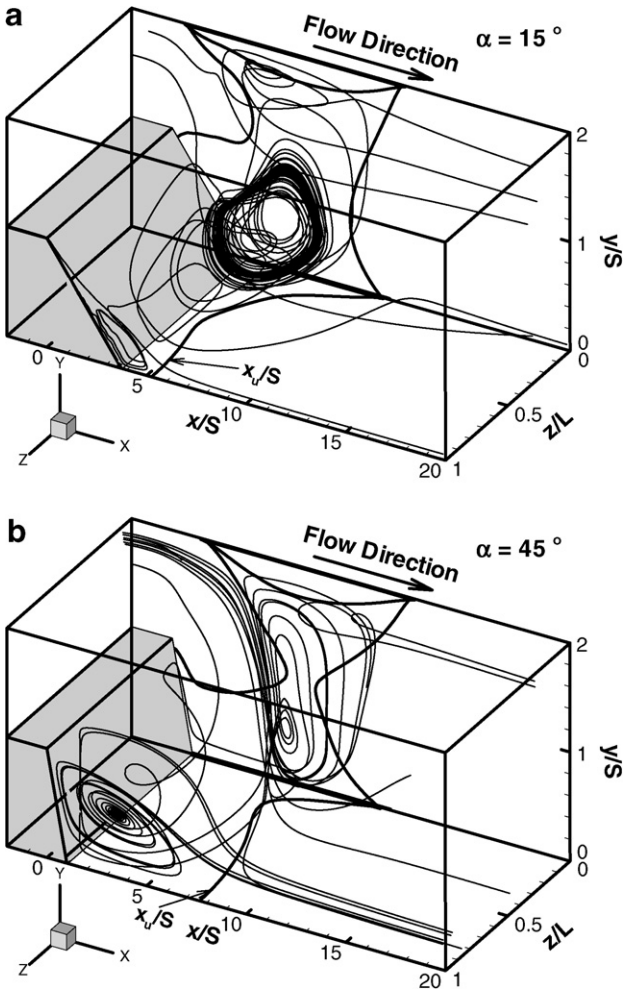

Fig. 3. General flow features adjacent to backward-facing step.

with a Reynolds number of 343. The flow conditions at the upstream inlet section of the duct ($x/S = -2$, $1 \leqslant y/S \leqslant 2$, for all z) are considered to be hydrodynamically steady and fully developed, and having uniform temperature profile ($T_0 = 20$ °C). Distribution of the mean stream-

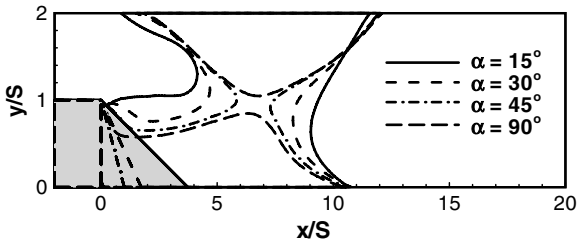

Fig. 4. Distribution of the x_u-lines adjacent to the sidewall ($z/L = 0.01$).

wise velocity component (u) is considered to be equivalent to the one described by Shah and London [19] and White [20] with the average inlet velocity of u_0:

$$u(y,z) = \frac{48u_0}{\pi^3\beta}\sum_{i=1,3,5,\ldots}^{\infty}(-1)^{(i-1)/2}\left\{1-\frac{\cosh[i\pi(z-L)/2L]}{\cosh(i\pi b/2L)}\right\} \times \frac{\cos[i\pi(y-b-S)/2L]}{i^3} \quad (6)$$

where $\beta = 1-\frac{192L}{\pi^5 b}\sum_{i=1,3,5,\ldots}^{\infty}\frac{\tanh(i\pi b/2L)}{i^5}$ and $b = h/2$. While the other velocity components (v and w) are set equal to zero at that inlet section ($x/S = -2$). Symmetry conditions were imposed at the center width of the duct ($z/L = 1$, for all x and y), and fully developed flow and thermal conditions were imposed at the exit section of the calculation domain ($x/S = 50$, for all y and z).

Numerical solution of the governing equations and boundary conditions was performed by utilizing SIMPLE algorithm [21] for the pressure correction in the iteration procedure. Hexahedron volume elements and non-uniform staggered grid arrangement are employed in the simulation. The grid is highly concentrated close to the step and near the corners, in order to ensure the accuracy of the numerical simulation. This flow simulation code was used in previous studies [12,13], and its description and validation can be found in these references. Grid independence tests were performed using several grid densities and distributions for the step inclination angle (α) of 90°, and the x_u-line which

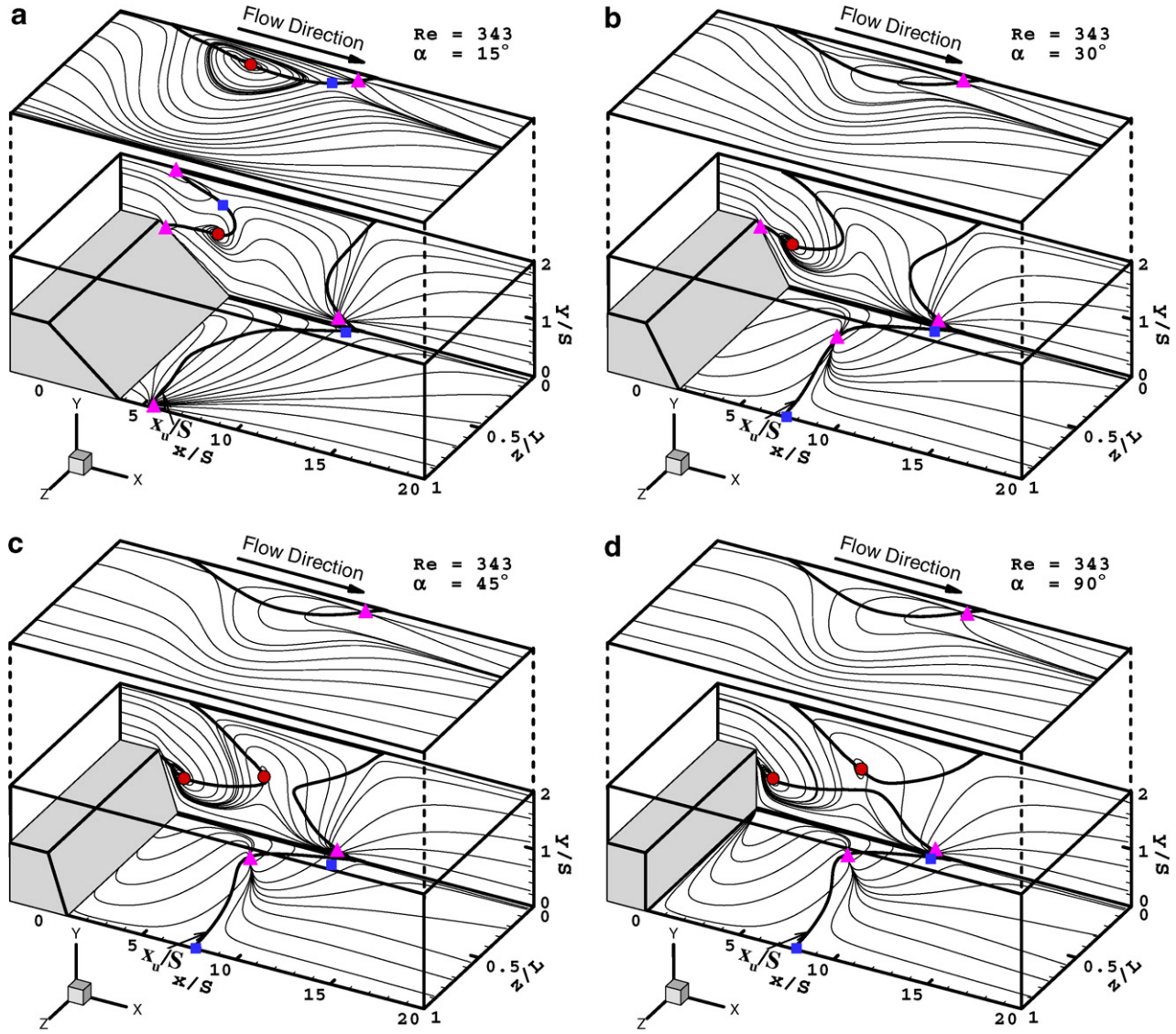

Fig. 5. Limiting streamlines adjacent to the bounding walls (●: foci; ▲: nodal; ■: saddle point).

designates the locations where the mean streamwise velocity component (u) is zero on a plane adjacent to the stepped wall was used as the criteria for grid independence solution. A grid of $180 \times 50 \times 36$ downstream from the step was selected for the simulation. Using a larger grid $200 \times 60 \times 42$ downstream from the step resulted in less than 2% difference in the predicted locations where the mean streamwise velocity component (u) is zero on a plane adjacent to the stepped wall. The residual sum for each of the conserved variables is computed and stored at the end of each iteration, thus recording the convergence history. The convergence criterion required that the maximum relative mass residual based on the inlet mass be smaller than 10^{-6}. Predictions of the locations where the mean streamwise velocity component (u) is zero on a plane adjacent to the stepped wall (line (x_u)) compare very well with laser-Doppler measured results [18] for $\alpha = 90°$, as shown in Fig. 2, and that provides code validation.

3. Results and discussion

Distributions of the x_u-lines adjacent to the stepped wall are shown in Fig. 2 for different step inclination angles. This line is a link of locations where the streamwise velocity component (u) is zero or changes its sign adjacent to the stepped wall. It is usually used as the reattachment location for 2-D flow in this geometry or at the center of the duct with very larger aspect ratio [12]. In 3-D case, the maximum length in its spanwise distribution appears at the sidewall ($z/L = 0$). As the step inclination angle (α) is greater than 45°, distributions of the x_u-lines are very close to each other, with the minimum to develop near the sidewall (at $z/L \approx 0.25$). Effects of the step inclination angle on the x_u-line distribution are not significant as $\alpha \geqslant 45°$. Hence, similar results for $\alpha = 60°$ will not be repeated in the following paragraphs due to space limitation. As the step inclination angle decreases, the x_u-line moves towards the downstream in the region near the sidewall ($z/L < 0.3$), while it becomes shorter in the region near the center width of duct ($0.3 < z/L < 1$). For $\alpha = 15°$, the x_u-line becomes more uniform near the center width of the duct and the minimum in its spanwise distribution is not very noticeable. The general behavior of the three-dimensional flow is shown in Fig. 3 through the presentations of streamlines that trace the paths of hypothetical massless particles placed in the flow field. Due to space limitations, the results that illustrate general flow features are presented only for the step inclination angles of $\alpha = 15°$ and 45°, and similar behavior develops for different step inclination angles. The general features of flow at $\alpha = 45°$ are similar to those at $\alpha = 90°$, which are described by Armaly et al. [11] and Nie and Armaly [12], including the swirling vertical flow inside the primary recirculation region, the reverse flow regions adjacent to the sidewall and the "jet-like" flow and its impingement on the stepped wall. At the step inclination angle of $\alpha = 15°$, the three-dimensionalities due to

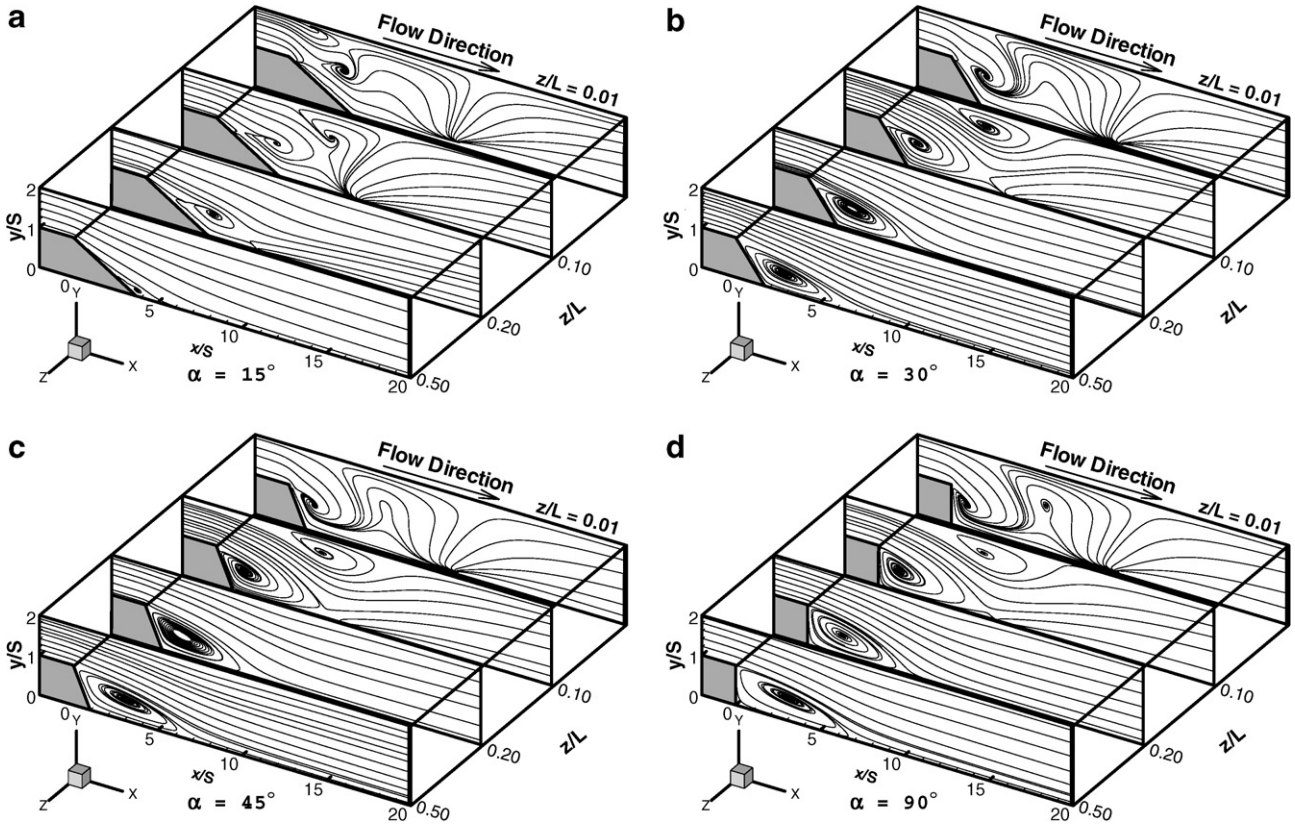

Fig. 6. Limiting streamlines at several z-planes.

sidewall are still significant. The reverse flow regions are observed near the sidewall with a larger size below the step and adjacent to the bottom wall. Streams from the lower portion of the sidewall reverse flow region flow toward the center width of the duct inside the primary recirculation region, and those from the upper portion flow toward the downstream in the region near the upper flatwall. The downwash near the sidewall and the step becomes stronger and the sidewall recirculation region moves further downstream as the step inclination angle increases. The size of the primary recirculation region which develops adjacent to the backward-facing step and the stepped wall becomes larger as the step inclination angle increases. Furthermore, the "jet-like" flow and its impingement which develop for the step inclination angle of $\alpha = 45°$ or higher are not observed for $\alpha = 15°$.

Distributions of the x_u-lines adjacent to the sidewall ($z/L = 0.01$) are presented in Fig. 4. This line is a link of points where the streamwise velocity component (u) is zero on the plane parallel and adjacent to the sidewall. Locations of these lines near the bottom wall ($y/S = 0$) are almost the same for different step inclination angles and they appear at $x/S \approx 11$ for this studied Reynolds number. The upstream and downstream edges of this line move closer to each other as the step inclination angle increases. They become connected as $\alpha = 90°$. It should be noted that this line represents the approximate size of the sidewall recirculation regions although it is not the actual boundaries of these recirculation regions [14]. The flow features can be seen more clearly from the limiting streamlines adjacent to the bounding walls, as shown in Fig. 5. The critical points including the foci, saddle and nodal points are also included in the figure. Streamlines projected onto a no-slip surface are the computational analogy to the experimental surface flow visualization [22]. The "jet-like" impingement location, which is a nodal point and the "source" of streamlines on the bottom wall, can be seen near the sidewall for the step inclination angles of $\alpha = 30°$, 45° and 90°. However, this does not appear on the stepped wall for the case of $\alpha = 15°$. Another feature of the x_u-line at the symmetry center of the duct ($z/L = 1$) is that it is a saddle point for the step inclination angles of $\alpha = 30°$, 45° and 90°, while

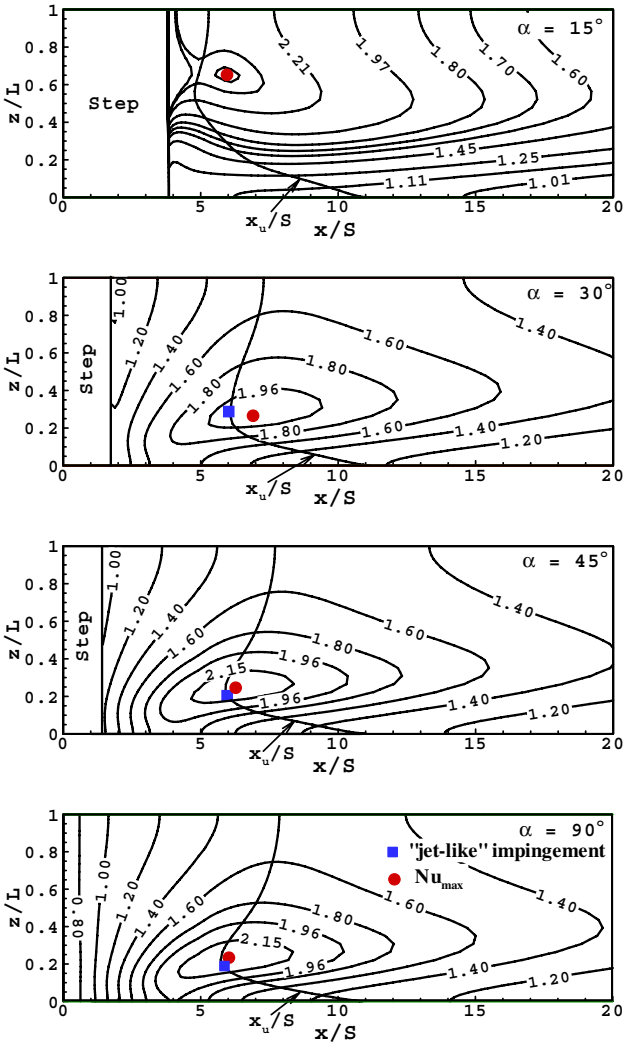

Fig. 7. Nusselt number distribution on the heated stepped wall.

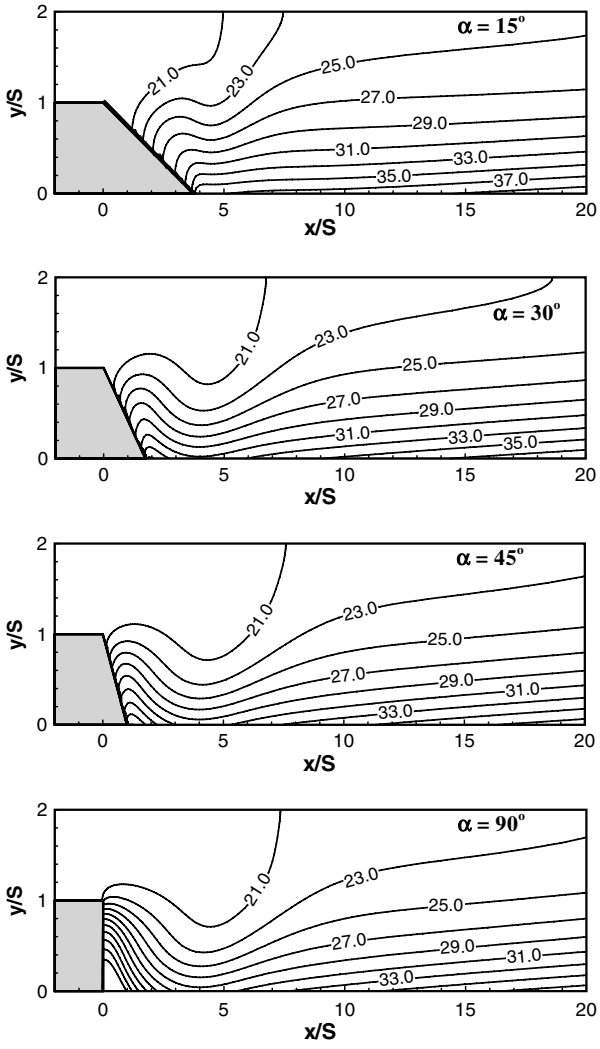

Fig. 8. Temperature distributions on the sidewall.

it is a nodal point for $\alpha = 15°$. The limiting streamlines on the sidewall exhibit that the downwash which develops near the sidewall because of sudden change in flow geometry becomes stronger as the step inclination angle increases. The recirculation region adjacent to the sidewall and near the separating edge of the step, which is in the counter-clockwise direction (viewed along the z-direction), moves towards the bottom wall as the step inclination angle increases. Another recirculation region which is in the clockwise direction (viewed along the z-direction) becomes larger in size as the step inclination angle increases. The reverse flow region near the upper flatwall for $\alpha = 15°$ is larger in the spanwise direction than that for $\alpha = 30°$. This is because of the longer "ramp" section for $\alpha = 15°$ compared with other step inclination angles. Streamlines at several intersections of z-planes are plotted in Fig. 6 for different step inclination angles. The reverse flow region adjacent to the flatwall develops only in the region close to the sidewall ($z/L \leqslant 0.1$). At the plane of $z/L = 0.5$, the primary recirculation region for $\alpha = 15°$ is much smaller than other step inclination angles.

Distributions of the Nusselt number (Nu) on the stepped wall are shown in Fig. 7. The dotted symbol denotes the location where the Nusselt number is maximum, and the square symbol represents the location where the "jet-like" flow impinges on the stepped wall. It should be noted that the Nusselt number is inversely proportional to the wall temperature on the stepped wall. The maximum Nusselt number develops near the sidewall (at $z/L \approx 0.25$), for the step inclination angles of $\alpha = 30°$–$90°$, as a result of the "jet-like" flow which develops near the sidewall and its impingement onto the stepped wall [11,12]. It appears downstream of the "jet-like" impingement location, and moves closer to the "jet-like" impingement location as the step inclination angle increases. The minimum Nusselt number is located near the backward-facing step for these step inclination angles ($\alpha \geqslant 30°$). However, for the step inclination angle of $\alpha = 15°$, the maximum Nusselt number is located near the center width of duct (at $z/L \approx 0.65$), as a result of strong downwash around this region. The minimum Nusselt number develops near the sidewall for this case. The maximum Nusselt number is 2.39, 2.04, 2.25 and 2.28 for the step inclination angles of $\alpha = 15°$, 30°, 45° and 90°, respectively. Temperature distributions on the sidewall are presented in Fig. 8. Near the backward-facing step, the wall temperature decreases as the step inclination angle increases because of the stronger downwash adjacent to the sidewall. Moreover, these temperature distributions show that the higher temperature develops near the corner where the backward-facing step and the bottom wall intersect, for the step inclination angles of $\alpha = 30°$–$90°$. However, this is not seen for the step inclination angle of $\alpha = 15°$.

Distributions of the friction coefficient (C_f) on the stepped wall are presented in Fig. 9. Locations of the maximum Nusselt number and the "jet-like" impingement are also included in order to show their relative positions.

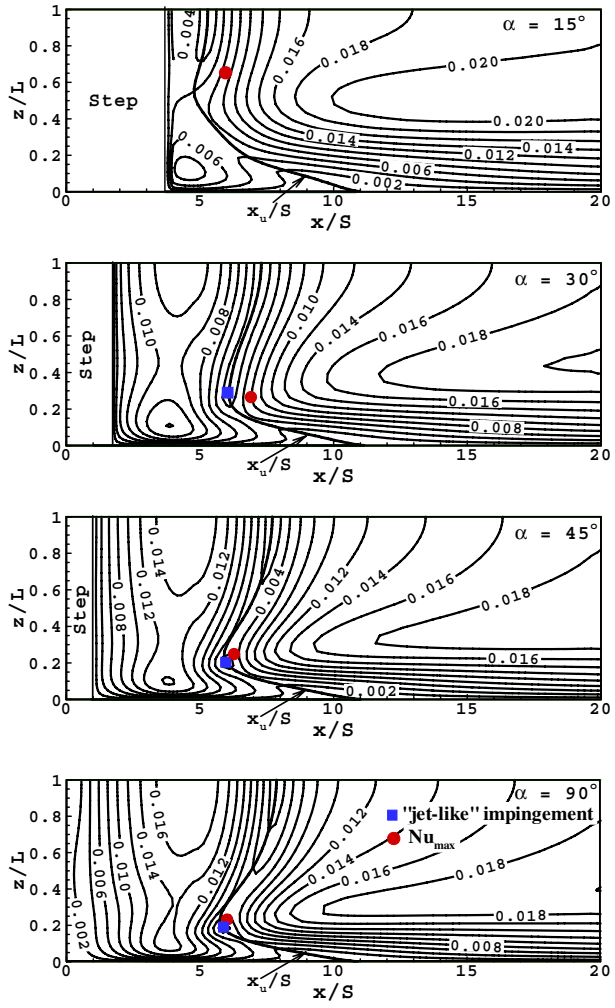

Fig. 9. Friction coefficient distribution on the stepped wall.

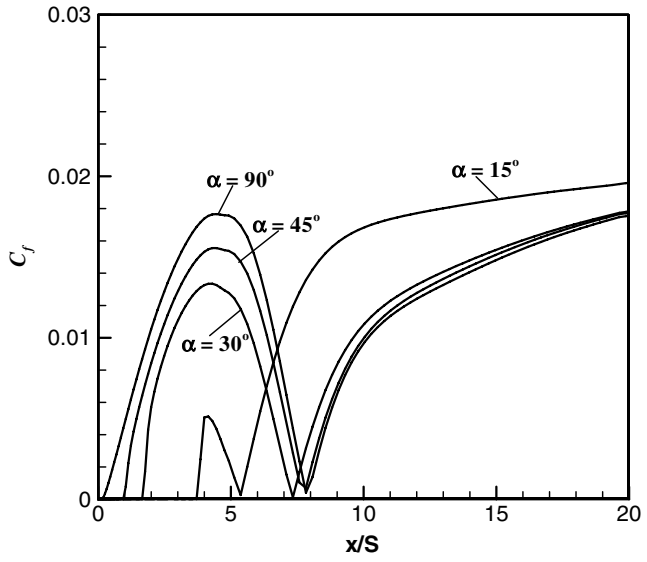

Fig. 10. Friction coefficient distribution along the center of the duct.

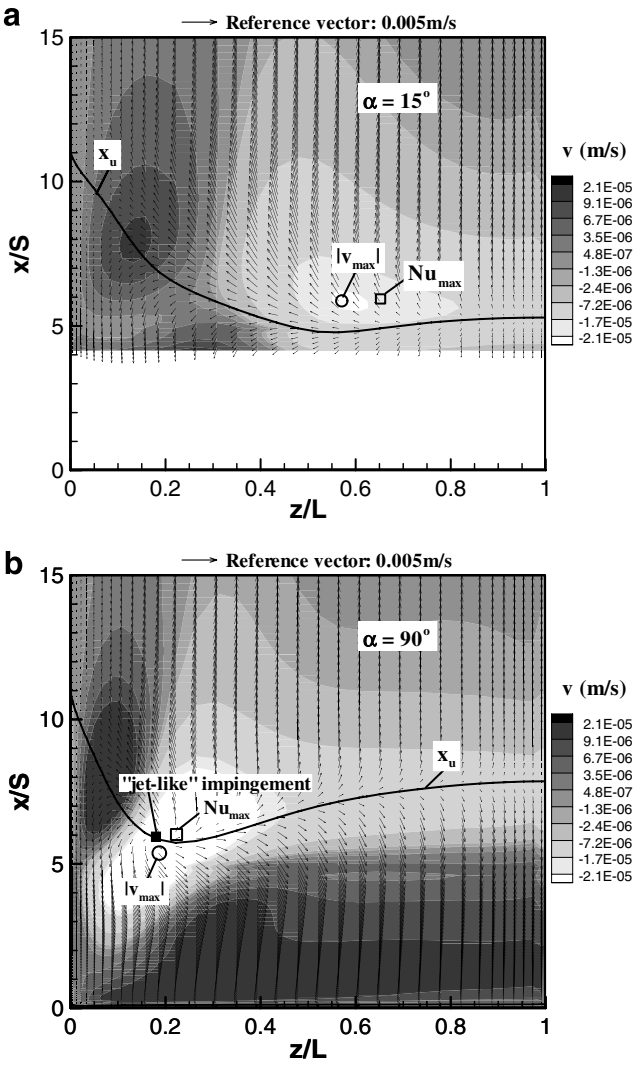

Fig. 11. Velocity vector field adjacent to the stepped wall.

The friction coefficient is low around the x_u-line. It has a minimum value at the "jet-like" impingement location, which develops for the step inclination angles of $\alpha = 30°$–90°. The magnitude of friction coefficient inside the primary recirculation region increases as the step inclination angle increases. This also can be seen from the friction coefficient distributions along the center width of the duct, as shown in Fig. 10. Downstream of the primary recirculation region, increase of the friction coefficient becomes slower as the step inclination angle increases.

Velocity vector field adjacent to the stepped wall is shown in Fig. 11. Contour lines of the normal velocity component to this wall (v) are also included in this figure. Different colors[1] represent different values of this velocity component. The circle symbol denotes the location where the magnitude of the negative v-velocity component (flow towards the bottom wall) is maximum. The square symbol represents the location where the Nusselt number is maximum. It can be seen that the flow away from the bottom wall (positive v-velocity component) is responsible for the maximum x_u-line to appear at the sidewall. This is because the positive v-velocity component (flow away from the bottom wall) lengthens the location of flow reattachment onto the stepped wall [12]. Fig. 11a shows that the maximum Nusselt number is closely associated with the negative v-velocity component, instead of the "jet-like" impingement, since it is not observed for the small step inclination angle such as $\alpha = 15°$.

[1] For interpretation of color in Fig. 11, the reader is referred to the web version of this article.

4. Conclusions

Results from numerical simulations of three-dimensional laminar forced convection flow adjacent to backward-facing step in a rectangular duct are used to examine effects of step inclination on the flow and heat transfer in this geometry. The "jet-like" flow and its impingement do not appear as the inclination angle of backward-facing step is small ($\alpha = 15°$). At the center of the duct ($z/L = 1$), the location where the streamwise velocity component is zero changes from a saddle point to a nodal point as the step inclination angle decreases. The downwash adjacent to the sidewall becomes stronger as the step inclination angle increases. The maximum Nusselt number on the stepped wall is located near the sidewall for $\alpha \geqslant 30°$ and it appears near the center of duct for small inclination angle ($\alpha = 15°$). Location of the maximum Nusselt number is closely associated with the location where the negative transverse velocity component is maximum. The friction coefficient inside the primary recirculation region increases with the increase of the step inclination angle. Downstream of the primary recirculation region, increase of the friction coefficient becomes slower as the step inclination angle increases.

Acknowledgement

This work was supported in part by the Army Research Laboratory under award DAAD 19-03-2-0007.

References

[1] B.F. Blackwell, B.F. Armaly (Eds.), Computational aspects of heat transfer – benchmark problems, HTD-vol. 258, American Society of Mechanical Engineers, New York, NY, 1993.
[2] B.F. Blackwell, D.W. Pepper (Eds.), Benchmark problems for heat transfer codes, HTD-vol. 222, American Society of Mechanical Engineers, New York, NY, 1992.
[3] J.L. Sohn, Evaluation of FIDAP on some classical laminar and turbulent benchmarks, Int. J. Numer. Methods Fluids 8 (12) (1988) 1469–1490.
[4] R.L. Simpson, Aspects of turbulent boundary-layer separation, Progress Aerospace Sci. 32 (5) (1996) 457–521.
[5] B.F. Armaly, F. Durst, J.C.F. Pereira, B. Schonung, Experimental and theoretical investigation of backward-facing step flow, J. Fluid Mech. 127 (1983) 473–496.

[6] J.K. Eaton, J.P. Johnson, A review of research on subsonic turbulent flow reattachment, AIAA J. 19 (9) (1981) 1093–1100.
[7] T.P. Chiang, T.W.H. Sheu, Vortical flow over a 3-D backward-facing step, Numer. Heat Transfer Part A – Applications 31 (2) (1997) 167–192.
[8] T.P. Chiang, T.W.H. Sheu, A numerical revisit of backward-facing step flow problem, Phys. Fluids 11 (4) (1999) 862–874.
[9] H. Iwai, K. Nakabe, K. Suzuki, Flow and heat transfer characteristics of backward-facing step laminar flow in a rectangular duct, Int. J. Heat Mass Transfer 43 (3) (2000) 457–471.
[10] D.B. Carrington, D.W. Pepper, Convective heat transfer downstream of a 3-D backward-facing step, Numer. Heat Transfer Part A – Applications 41 (6–7) (2002) 555–578.
[11] B.F. Armaly, A. Li, J.H. Nie, Three-dimensional forced convection flow adjacent to backward-facing step, AIAA J. Thermophys. Heat Transfer 16 (2) (2002) 222–227.
[12] J.H. Nie, B.F. Armaly, Reattachment of three-dimensional flow adjacent to backward-facing step, ASME J. Heat Transfer 125 (3) (2003) 422–428.
[13] J.H. Nie, B.F. Armaly, Three-dimensional convective flow adjacent to backward-facing step – effects of step height, Int. J. Heat Mass Transfer 45 (12) (2002) 2431–2438.
[14] J.H. Nie, B.F. Armaly, Reverse flow regions in three-dimensional backward-facing step flow, Int. J. Heat Mass Transfer 47 (22) (2004) 4713–4720.
[15] H. Iwai, K. Nakabe, K. Suzuki, K. Matsubara, The effects of duct inclination angle on laminar mixed convective flows over a backward-facing step, Int. J. Heat Mass Transfer 43 (3) (2000) 473–485.
[16] A. Li, B.F. Armaly, Laminar mixed convection adjacent to three-dimensional backward-facing step, ASME J. Heat Transfer 124 (1) (2002) 209–213.
[17] J.G.B. Saldana, N.K. Anand, V. Sarin, Numerical simulation of mixed convective flow over a three-dimensional horizontal backward facing step, ASME J. Heat Transfer 127 (9) (2005) 1027–1036.
[18] B.F. Armaly, A. Li, J.H. Nie, Measurements in three-dimensional separated flow, Int. J. Heat Mass Transfer 46 (19) (2003) 3573–3582.
[19] R.K. Shah, A.L. London, Laminar Forced Convection in Ducts, Academic Press, New York, NY, 1978.
[20] F.M. White, Viscous Fluid Flow, McGraw-Hill, New York, NY, 2005.
[21] S.V. Patankar, Numerical Heat Transfer and Fluid Flow, Hemisphere, New York, NY, 1980.
[22] A.E. Perry, M.S. Chong, Interpretation of flow visualization, in: A.J. Smits, T.T. Lim (Eds.), Flow Visualization: Techniques and Examples, Imperial College Press, London, UK, 2000, pp. 1–26.